ISPRS Annals of the Photogrammetry, Remote Sensing and Spatial Information Sciences, Volume X-5/W4-2025
Philippine Geomatics Symposium (PhilGEOS) 2025 "Enhancing Human Quality of Life through Geospatial Technologies",
24–25 November 2025, Quezon City, Philippines

Correlation of Land Subsidence with Groundwater Extraction and Urbanization in Hagonoy and Calumpit, Bulacan from 2015 to 2021-Q1

John Dave C. Maclang [1,2], Alexi Mae Y. Narca [1,2], Rosalie B. Reyes [1,2], Luis Carlos S. Mabaquiao [1,2]

[1] Department of Geodetic Engineering, University of the Philippines Diliman
[2] Training Center for Applied Geodesy and Photogrammetry, University of the Philippines, Diliman, Quezon City, Philippines - (jcmaclang, aynarca, rbreyes3, lsmabaquiao)@up.edu.ph

Keywords: Geographically Weighted Regression, Ordinary Least Squares, Persistent Scatterer Interferometry, Groundwater Extraction, Land Deformation.

Abstract

This study investigates the spatial relationship between land subsidence and the patterns of groundwater extraction and urbanization in Hagonoy and Calumpit, Bulacan, from 2015 to the first quarter of 2021. Using Persistent Scatterer Interferometry (PSI) from Sentinel-1 InSAR data, zonal proximity analysis, and spatial regression techniques, the research quantifies deformation patterns and their association with anthropogenic stressors. Ordinary Least Squares (OLS) and Geographically Weighted Regression (GWR) models assessed the explanatory power of groundwater level (GWL), population density, and built-up volume. GWR on grid-based PSI sampling outperformed OLS with an adjusted R^2 of 0.88, capturing localized subsidence drivers. Results revealed subsidence rates reaching -124.51 mm/year near high-extraction zones. Areas within 500 meters of pumping stations exhibited significantly higher deformation (mean: -70.22 mm/year) than more distant areas (-65.31 mm/year), as confirmed by Welch's t-tests ($p < 0.001$). Estimates show that Hagonoy's annual extraction volume (~9 million m^3) may contribute -81 mm/year of subsidence. Findings highlight the urgent need for localized monitoring, improved input data from water utilities and Philippine Statistics Authority (PSA), and integration of subsidence risk into land-use planning. The study demonstrates the effectiveness of spatial modeling in understanding land deformation processes in data-limited, flood-prone coastal municipalities.

1. Introduction

1.1 Background

Land subsidence, the gradual sinking of the earth's surface, became a critical issue in many rapidly urbanizing regions, which can be caused by human activities like groundwater, oil, or gas extraction, fracking, and mining, as well as from natural processes, including earthquakes, soil compaction, glacial isostatic adjustment, erosion, sinkhole formation, and the saturation of wind-deposited fine soils (NOAA, 2024). As urban populations grew, the rising demand for groundwater intensified pressure on aquifers, leading to ground deformation (Velis et al., 2017; Dang et al., 2014).

Despite the growing awareness of land subsidence as a global issue, there remains a significant gap in understanding the specific dynamics of this phenomenon in local contexts. Although studies have documented the impact of groundwater extraction on subsidence in large cities, less is known about how these dynamics affect smaller urbanizing areas. The low-lying municipalities of Hagonoy and Calumpit, Bulacan, in the Philippines face similar challenges. The persistent flooding issues in these municipalities highlight the need for localized research. Despite Bulacan's proximity to Angat Dam, and even the Ipo Dam and Bustos Dam, numerous households in the province relied heavily on deep wells drawing on groundwater sources for domestic and municipal uses due to limited water rights (Fresco, 2012). This dependence on groundwater placed a heightened risk of land subsidence, which led to a decrease in ground elevation that creates a basin-like area prone to flooding (Lagos et al., 2023).

1.2 Objectives and Significance

This study aims to bridge the knowledge gap by examining the relationship between land subsidence, groundwater extraction, and urbanization in Hagonoy and Calumpit, Bulacan, from 2015 to the first quarter of 2021. It utilizes Sentinel-1 Persistent Scatterer Interferometric Synthetic Aperture Radar (PSI-InSAR) data to measure ground deformation rates, historical groundwater records from local water management authorities, and urbanization data from the Global Human Settlement Layer (GHSL) alongside records of active household service connections.

This paper specifically seeks to analyze patterns of land subsidence in relation to groundwater levels (GWLs), proximity to extraction zones, population density, and built-up surface volume. It applies GIS-based spatial analysis to evaluate how groundwater availability and extraction influence ground deformation. Furthermore, it aims to determine the combined explanatory power of GWL, built-up volume, and population density on subsidence rates through Ordinary Least Squares (OLS) regression, and to assess localized spatial variations using Geographically Weighted Regression (GWR). Through these analyses, the study evaluates the extent of ground-level changes and examines how these shifts are associated with potential drivers, contributing to a deeper understanding of their impact on ground stability in the area.

The findings are expected to provide critical insights into the underlying causes of land subsidence in Hagonoy and Calumpit. By identifying the key spatial factors influencing ground deformation, the study can inform local government units, water resource managers, and policymakers in crafting targeted mitigation strategies and land-use planning frameworks. Ultimately, the results aim to support broader efforts in sustaining groundwater resources and minimizing geohazard risks, particularly in less urbanized and vulnerable areas.

1.3 Scope and Limitations

The municipalities of Hagonoy and Calumpit, Bulacan, including Barangay San Isidro II in Paombong. It examined land subsidence patterns from 2015 to 2021-Q1 using Sentinel-1A and 1B PSI InSAR data. It analyzes the relationship between land

This contribution has been peer-reviewed. The double-blind peer-review was conducted on the basis of the full paper.
https://doi.org/10.5194/isprs-annals-X-5-W4-2025-307-2026

subsidence and two primary factors: groundwater extraction and urbanization. Ground deformation was correlated with GWL and urbanization patterns based on built-up volume and population density data from the GHSL. Service connection records were also used to supplement the urbanization analysis with localized indicators of water demand.

The study is limited to the influence of groundwater extraction and urban development on land subsidence. Other possible contributing factors, such as geological structure, soil compaction, tectonic activity, and surface loading, were outside the scope. Data availability was also a constraint, particularly for historical groundwater extraction records and high-resolution demographic data, which required the use of estimation methods and global datasets.

Despite these limitations, the study provides valuable insights into land subsidence dynamics in groundwater-dependent areas and contributes to broader efforts aligned with Sustainable Development Goals (SDGs) 11 (Sustainable Cities and Communities) and 13 (Climate Action).

2. Materials and Methods

2.1 Study Area and Data Collection

The municipalities of Hagonoy and Calumpit experienced growing urbanization and heavy reliance on groundwater extraction. Additionally, both towns were naturally prone to flooding, where even regular high tides can result in inundation (Cos, 2020). These conditions made the municipalities critical areas for examining the interaction between land subsidence, urbanization, and groundwater extraction in Bulacan.

Figure 1 presents the spatial distribution of subsidence points and their proximity to groundwater pumping stations, highlighting areas potentially affected by extraction activities.

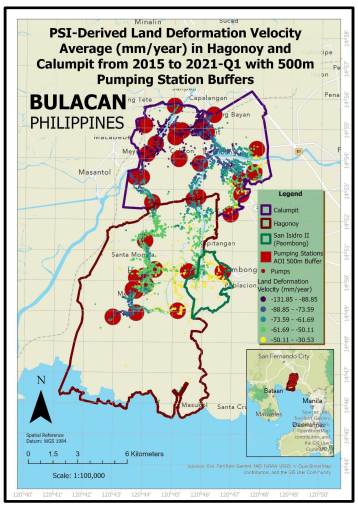

Figure 1. Subsidence points classified by average velocity (mm/year), overlaid with 500-meter buffers around pumping stations in Hagonoy, Calumpit, and part of Paombong.

This study analyzed land subsidence using PSI data derived from Sentinel-1A and 1B satellites. The datasets, generated under the EMSN091 activation through the Copernicus Emergency Management Service and produced by Indra Sistemas in collaboration with Gisat, covered 2014-2021 for the descending track and 2017-2021 for the ascending track, offering point-based velocity measurements in millimeters per year (EC and JRC, 2021a).

Urbanization data from the 2020 GHSL (GHS-BUILT-V and GHS-POP products at ~90-meter resolution) provided estimates of built-up volume (BUILTV2020) and gridded population density (GHSLPOP2020), which were used as explanatory variables for subsidence modeling (EC and JRC, 2021b).

Groundwater extraction data, including pumping station locations and SWL, were gathered from local water districts, the Mines and Geosciences Bureau (MGB), and the National Water Resources Board (NWRB). As historical SWL data before 2020 were unavailable, GWLs for 2015-2021 were approximated by interpolating 2020-2024 SWL records using ordinary kriging. GWL surfaces were derived by subtracting SWL from the 30-meter SRTM DEM. While this approach assumes a relatively linear trend in groundwater changes over time and provides reasonable local estimates, it introduces uncertainty by potentially smoothing short-term fluctuations at individual pumping sites, which may locally influence subsidence patterns.

This GWL surface, along with urbanization and groundwater extraction data, was used in the GWR analysis to examine subsidence drivers. The study acknowledges the vertical variations inherent in SRTM DEMs due to their surface-based representation and considers them suitable for the relatively low urban density of the study area.

2.2 Data Processing and Analysis

Following the general workflow (Figure 2), data processing and analysis began with compiling groundwater extraction, PSI land deformation velocity, and urbanization datasets. Preprocessed layers were prepared for value extraction, including the calculation of Distance-Weighted Average (DWA) extraction values. These datasets were integrated into a master shapefile, forming the basis for subsequent spatial and statistical analyses.

Initial spatial autocorrelation tests were performed using Global and Local Moran's I to assess the clustering patterns of land subsidence. Significant hotspots were identified through Getis-Ord Gi* cluster and hot spot analysis. These preliminary results provided insights into the spatial distribution of ground deformation. To model the relationship between land subsidence (LS) and potential explanatory variables, OLS regression was implemented. The model incorporated groundwater extraction (GWE), groundwater level (GWL), built-up volume (BUV), and population density (POP). Model diagnostics, including the Variance Inflation Factor (VIF), Jarque-Bera, Koenker BP, and Moran's I tests, were applied to assess multicollinearity, residual normality, heteroskedasticity, and spatial autocorrelation.

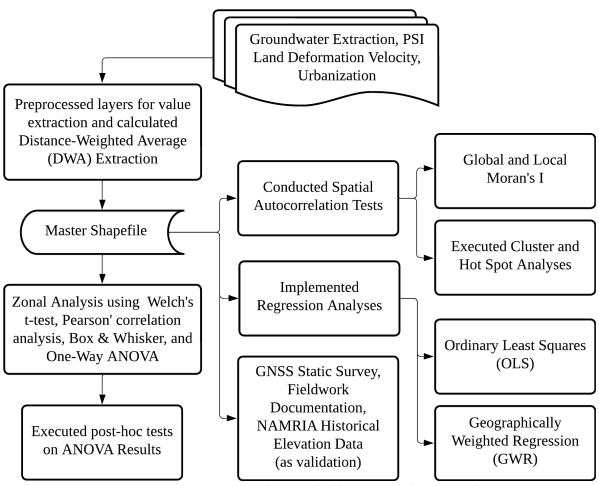

Figure 2. General workflow of the study.

This contribution has been peer-reviewed. The double-blind peer-review was conducted on the basis of the full paper.
https://doi.org/10.5194/isprs-annals-X-5-W4-2025-307-2026 | © Author(s) 2026. CC BY 4.0 License.

Given the spatial heterogeneity observed, GWR was applied to capture local variations in the influence of GWL, population density, and built-up volume on subsidence. Groundwater extraction was excluded from GWR due to multicollinearity. Moran's I was also used to check residual spatial autocorrelation in the GWR outputs.

Urbanization metrics were extracted using GHSL-built and GHSL-population raster datasets clipped to the study area. Service connection data from 2015 to 2024 were analyzed to evaluate trends in water demand, complementing groundwater extraction data. Missing extraction records from 2015 to 2019 were proportionally estimated based on the 2020 reported data.

Further zonal analysis was conducted by delineating extraction influence zones based on proximity to groundwater pumping stations. PSI points were classified using two schemes: a linear zoning with 250-meter intervals (PZ1-PZ5) and a non-linear zoning designed to capture the rapid decay of extraction effects, defined as 0-100 m (PZ1), 101-300 m (PZ2), 301-600 m (PZ3), 601-1000 m (PZ4), and beyond 1000 m (PZ5). Subsidence rates across zones were compared using Welch's t-tests, Pearson's correlation analysis, Box and Whisker plots, and one-way ANOVA, with post hoc tests (LSD, HSD, Scheffé) employed to assess pairwise differences.

To address the uneven distribution of PSI points and avoid spatial bias, a fishnet-based sampling strategy was applied by generating uniform 250-meter grids across the study area. Within each grid, one representative PSI point was selected based on deformation velocity. After testing maximum, minimum, and average values, the minimum velocity was chosen as it captures the highest rate of subsidence and reflects the worst-case ground movement scenario. This approach aligned with the study's focus on hazard identification, ensuring that the most critical deformation signals were represented while maintaining a spatially balanced dataset for analysis.

The sampled datasets were then utilized in OLS modeling, allowing a more representative evaluation of the relationship between land subsidence and groundwater extraction.

Finally, GNSS field surveys were conducted on recovered ground control points (GCPs) to validate PSI-derived subsidence velocities. Elevation differences between historical and current GNSS measurements were used to estimate ground displacement rates, which were compared against PSI data to verify the rates of land subsidence.

The regression model used to quantify LS was represented by the following equation:

$$LS=\beta_0+1(GWE)+2(GWL)+3(POP)+4(BUV)+\epsilon, \quad (1)$$

where LS = land subsidence rate
GWE = DWA extraction
GWL = groundwater level
POP = GHSL population density
BUV = Built-up volume
β_0 = Model intercept
ϵ = Model's random error (residual) term

3. Results and Discussion

3.1 Results of Land Subsidence Analyses

3.1.1 Spatial Patterns of Land Subsidence

The most severe subsidence rates from PSI data (Figure 3), reaching -131 mm/year, occurred in southern Hagonoy and central Calumpit, while coastal areas near Manila Bay showed moderate to low subsidence.

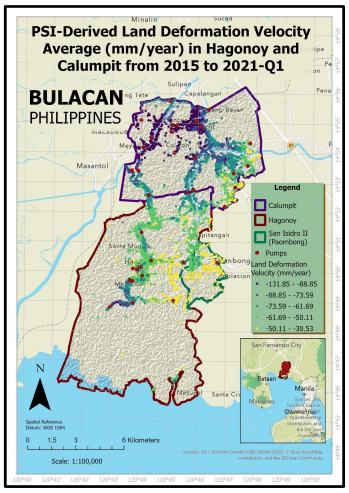

Figure 3. PSI-derived land deformation velocity average (mm/year) in Hagonoy and Calumpit from 2015 to 2021-Q1.

PSI-derived subsidence data (Figure 4) revealed spatial clustering in Hagonoy and Calumpit. Local Moran's I identified high-high clusters in central and southern Hagonoy and parts of Calumpit, and low-low clusters in less urbanized northern Calumpit. Getis-Ord Gi* confirmed these patterns, detecting 99% confidence hotspots near extraction sites and urban areas, and cold spots in sparsely developed zones. These results highlighted the spatial heterogeneity and temporal persistence of subsidence, supporting the link between groundwater extraction, urbanization, and ground deformation.

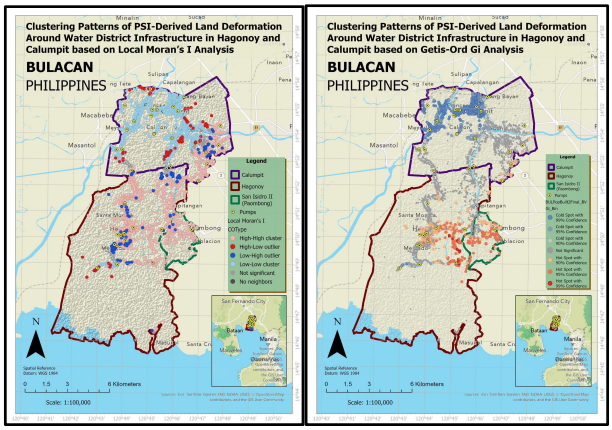

Figure 4. Clustering patterns of PSI-derived land deformation around water district infrastructure in Hagonoy and Calumpit based on Local Moran's I and Getis-Ord Gi analysis.

3.1.2 Temporal Patterns of Land Subsidence

Time series graphs (Figure 5) show ground deformation trends at PSI points nearest to each pumping station in Hagonoy and Calumpit. It showed consistent subsidence trends from 2017 to 2020, with maximum displacements of -350 mm in Hagonoy and -500 mm in Calumpit. Variations in subsidence rates reflected differences in groundwater extraction, geology, or surface loading, offering localized insights into broader land deformation patterns.

This contribution has been peer-reviewed. The double-blind peer-review was conducted on the basis of the full paper.
https://doi.org/10.5194/isprs-annals-X-5-W4-2025-307-2026 | © Author(s) 2026. CC BY 4.0 License.

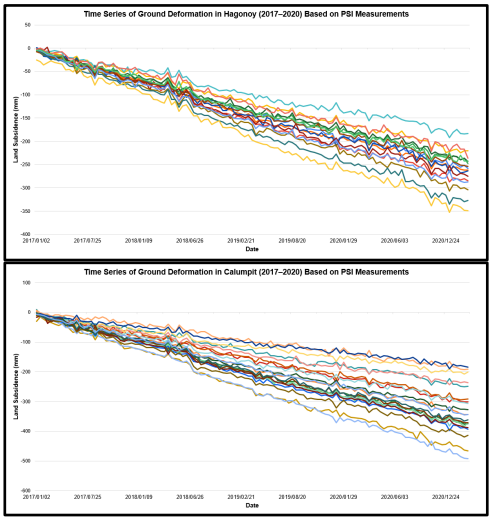

Figure 5. Time series of ground deformation in Hagonoy and Calumpit (2017-2020) based on PSI measurements.

3.1.3 Validation of Land Subsidence Data

To validate the PSI-derived subsidence measurements, GNSS surveys were conducted at six recovered GCPs in Hagonoy and Calumpit. Table 1 compares average velocities from PSI points and GNSS measurements at these locations.

GCPs	Distance to Nearest PSI Point (m)	Nearest PSI Average Velocity (mm/yr)	GNSS Average Velocity (mm/yr)
BLN 14	69.613	-40.446	-55.060
BLN 15	54.454	-79.468	-73.712
BL 362	7.663	-89.739	-76.483
BLN 50	28.744	-59.533	-60.385
BLN 3071	41.114	-52.626	-60.529
BLN 3120	70.957	-60.210	-49.824

Table 1. Comparison of subsidence velocities from PSI and GNSS measurements at GCPs in Hagonoy and Calumpit.

Table 1 shows that both PSI and GNSS datasets recorded negative velocities, confirming ongoing subsidence. Although differences in subsidence rates existed, the overall trend confirmed persistent ground deformation across the study area. A scatterplot comparison (Figure 6) yielded a coefficient of determination (R^2) of 0.704, indicating a strong positive correlation.

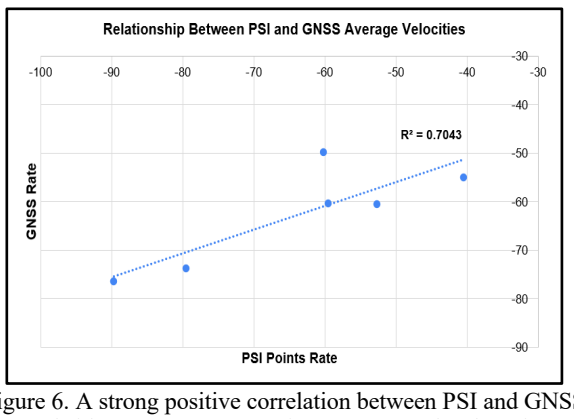

Figure 6. A strong positive correlation between PSI and GNSS subsidence measurements in Hagonoy and Calumpit

This strong correlation reinforced the consistency between PSI and GNSS measurements, validating the use of PSI data for regional-scale deformation monitoring. The combination of PSI's broad spatial coverage and the localized accuracy of GNSS strengthens confidence in the observed patterns of land subsidence from 2015 to 2021.

Beyond the numerical validation, field observations provided additional evidence of land subsidence impacts. In Hagonoy and Calumpit, visible signs of ground deformation were documented, including differences in height references on utility posts, abandoned and submerged houses, frequent road-raising projects, and structural adaptations in public buildings and vehicles. These on-ground observations offer a tangible representation of the trends captured by PSI and GNSS analyses.

Figure 7 showed older utility poles embedded deeper than newer ones, indicating ground lowering. Figure 8 highlights flood adaptations, such as an elevated tricycle and a flooded high school in Calumpit, showing subsidence's long-term impact on infrastructure. These observations validate PSI measurements, demonstrating persistent land deformation in Hagonoy and Calumpit.

Figure 7. Comparison of height references between an old and newer post in Hagonoy, Bulacan, showing deeper ground embedding of the older post based on 5-ft. marks.

Figure 8. Flood adaptations: elevated tricycle in Hagonoy and a flooded high school in Calumpit with inaccessible classrooms.

3.2 Groundwater Extraction Patterns

3.2.1 Trends in Groundwater Extraction

Groundwater extraction trends from 2015 to 2024 (Figure 9) revealed distinct patterns in Hagonoy and Calumpit. In Hagonoy, most pumping stations, such as Sta. Monica, San Agustin, and San Pedro showed rising extraction volumes likely driven by urbanization, while a few, like Old Poblacion and San Isidro, remain stable or decline. In Calumpit, extraction patterns are more varied, with stations like Buguion and Meysulao showing decreasing volumes, while Balungao and Caniogan exhibited steady or increasing rates. Local water district data indicated declining extraction in several stations, which may have reflected eventual closure potentially linked to reduced well productivity or aquifer depletion. Overall, extraction in Calumpit was lower than in Hagonoy, likely due to a combination of regulatory

controls, unaccounted alternative water sources, or localized aquifer depletion.

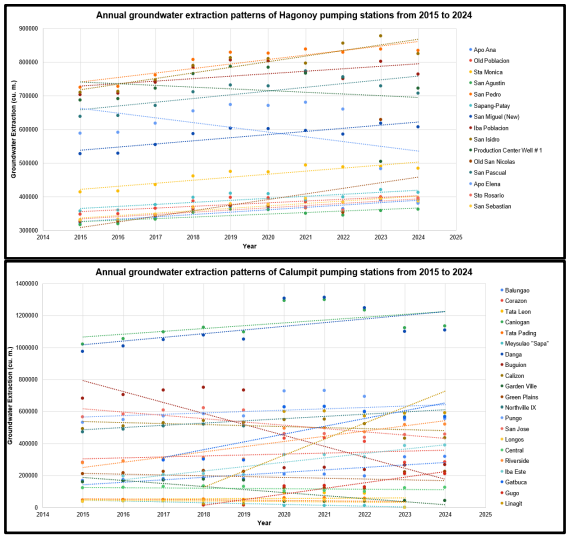

Figure 9. Annual groundwater extraction patterns of Hagonoy and Calumpit pumping stations from 2015 to 2024.

3.2.2 Groundwater Extraction and Subsidence Relationship

Time-series comparisons between groundwater extraction and land subsidence rates from 2017 to 2020 showed a strong inverse relationship in both municipalities (Figure 10).

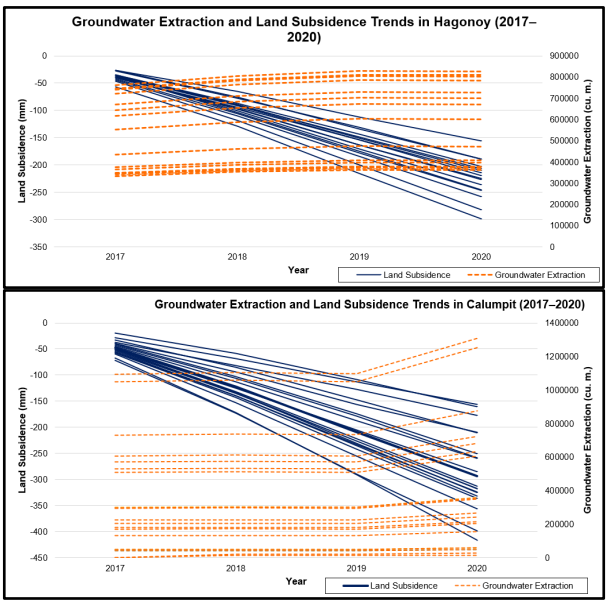

Figure 10. Groundwater extraction and nearest land subsidence trends in Hagonoy and Calumpit from 2017 to 2020.

Time-series comparisons between groundwater extraction and land subsidence rates from 2017 to 2020 showed a strong inverse relationship in both municipalities (Figure 10).

Most stations in Hagonoy and Calumpit exhibited strong negative correlations ($r \approx -0.76$ to -0.89). In Hagonoy, stations like Old Poblacion and Mercado had particularly high correlations ($r \approx -0.89$), while Gugo and Linagit in Calumpit showed similar patterns.

These negative correlations showed that as extraction volumes increased, subsidence rates also intensified. Variations across stations suggest that even moderate extraction in sensitive areas can cause significant deformation. Persistent subsidence despite reduced extraction indicated delayed compaction effects or local aquifer conditions. While uncertainties remain due to estimated data, the trends highlighted the need for stricter groundwater regulation and monitoring to mitigate future subsidence risks in Bulacan.

3.3 Service Coverage, Extraction Volume, and GWL

3.3.1 Spatial Distribution of GWLs

Figure 11 presents the spatial distribution of estimated GWL across Hagonoy, Calumpit, and part of Paombong. Deeper GWLs are concentrated in southern and central Hagonoy, while shallower levels are found in northern Calumpit and Paombong. Overlaying the GWL surface with subsidence data reveals that areas with deeper GWLs tended to coincide with higher rates of deformation, which suggests a potential link between groundwater stress and land subsidence. However, spatial variability indicated that other factors, such as soil properties and historical extraction, also contribute to subsidence patterns.

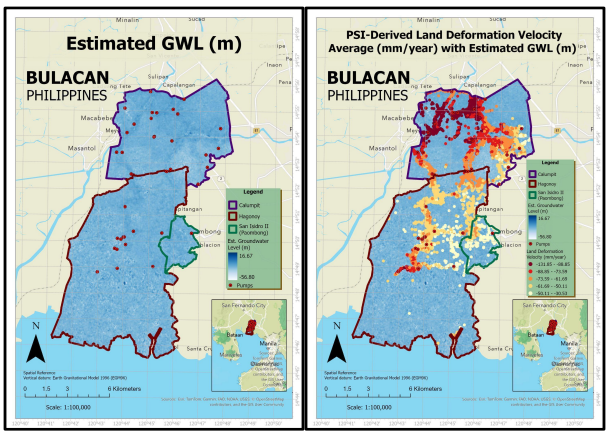

Figure 11. Estimated GWL of the study area.

3.3.2 Relationship Between Service Connections and Groundwater Extraction

Figure 12 shows trends in service connections and groundwater extraction in Hagonoy and Calumpit. In Hagonoy, both variables rose steadily from 2015 to 2019, driven by urbanization, before extraction rates stabilized while service connections continued to grow. The Pearson correlation of 0.815 confirmed a strong relationship. In Calumpit, both variables grew until 2018, after which extraction stabilized but service connections kept rising, with a stronger correlation of 0.873.

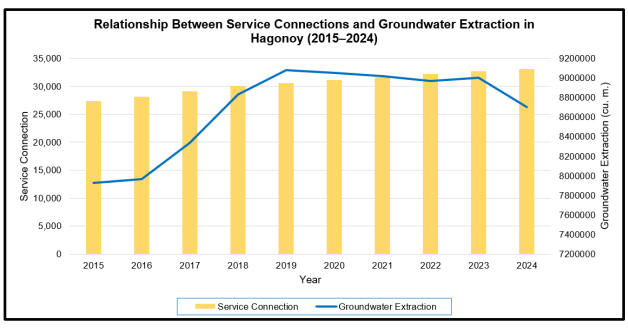

This contribution has been peer-reviewed. The double-blind peer-review was conducted on the basis of the full paper.
https://doi.org/10.5194/isprs-annals-X-5-W4-2025-307-2026 | © Author(s) 2026. CC BY 4.0 License.

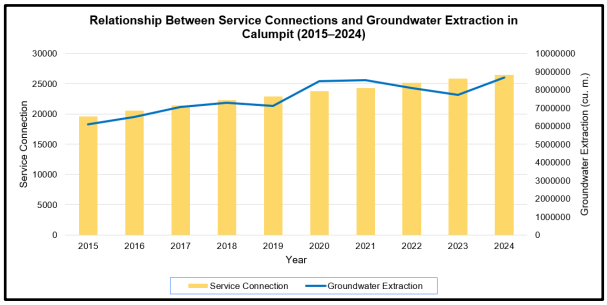

Figure 12. Relationship between service connections and groundwater extraction in Hagonoy from 2015 to 2024.

These strong spatial and statistical relationships suggested that groundwater extraction significantly contributes to subsidence risk, particularly in areas with deeper GWLs. The divergence between service connection growth and extraction rates in recent years pointed to potential improvements in water management.

3.4 Regression Modeling: OLS and GWR Results

3.4.1 Pre-Model Diagnostics and Data Reliability Assessment

Prior to regression analysis, diagnostic tests were conducted to assess model suitability. Global Moran's I revealed significant spatial clustering in both LS and all predictors, indicating potential spatial autocorrelation. Linearity checks showed weak global associations ($R^2 < 0.10$) between subsidence velocity and most predictors, supporting the use of GWR to capture spatially varying relationships. Multicollinearity diagnostics showed all VIF values below the threshold (with values ranging from 1.005 - 1.137), ensuring model stability. The global OLS yielded an adjusted R^2 of 0.146 and a Corrected Akaike Information Criterion (AICc) of 38759.86 for the full PSI dataset.

3.4.2 OLS Model Results

Despite significant coefficients, diagnostic tests revealed OLS assumption violations. Heteroskedasticity and non-normal residuals were detected. While the large sample size lessens concerns about non-normality affecting estimates, these deviations may still reflect model misspecification. Spatial autocorrelation in residuals indicated the OLS model failed to capture spatial heterogeneity, motivating GWR.

Table 2 shows coefficients, p-values, and adjusted R^2 for OLS models across Hagonoy, Calumpit, and the AOI using different PSI selections. All models had negative intercepts, especially in Calumpit, suggesting baseline subsidence from unaccounted factors like soil compaction and historical extraction.

	COEFFICIENT β					ROBUST VALUE					
	WHOLE AOI					WHOLE AOI					
FACTORS	intercept	dwa_extrac	gwl	ghsl_pop	builtv	intercept	dwa_extrac	gwl	ghsl_pop	builtv	R^2 Values
All points	-101.14694	0.000003	-1.814271	0.022523	-0.000449	0.000000*	0.001128*	0.000000*	0.000000*	0.000000*	0.145943
250_min	-100.295656	-0.000003	-1.694482	0.022518	-0.000701	0.000000*	0.132046	0.000000*	0.000036*	0.000000*	0.122341
250_max	-101.033962	-0.000001	-1.987219	0.024307	-0.000307	0.000000*	0.534311	0.000000*	0.000051*	0.000149*	0.115108
150_min	-100.522637	-0.000002	-1.728205	0.021279	-0.000571	0.000000*	0.220739	0.000000*	0.000038*	0.000000*	0.12004
150_max	-101.288586	-0.000001	-1.894931	0.02402	-0.00033	0.000000*	0.8762	0.000000*	0.000014*	0.000001*	0.106748
	HAGONOY					HAGONOY					
FACTORS	intercept	dwa_extrac	gwl	ghsl_pop	builtv	intercept	dwa_extrac	gwl	ghsl_pop	builtv	R^2 Values
All points	-37.461143	-0.000003	0.833099	0.005163	-0.00051	0.000000*	0.005718*	0.000000*	0.030417*	0.000000*	0.105343
250_min	-38.55608	-0.000009	0.63951	0.0069	-0.001351	0.000000*	0.002307*	0.049527*	0.222777	0.000000*	0.261838
250_max	-35.469696	-0.000003	0.664531	0.006914	-0.000591	0.000000*	0.151979	0.005742*	0.116451	0.000004*	0.112485
150_min	-36.283391	-0.000006	0.76787	0.00461	-0.001157	0.000000*	0.003043*	0.000851*	0.327587	0.000000*	0.244276
150_max	-34.210719	-0.000003	0.808231	0.006664	-0.00063	0.000000*	0.061534	0.000016*	0.143878	0.000000*	0.117717
	CALUMPIT					CALUMPIT					
FACTORS	intercept	dwa_extrac	gwl	ghsl_pop	builtv	intercept	dwa_extrac	gwl	ghsl_pop	builtv	R^2 Values
All points	-123.682247	0.000004	-2.338562	0.025646	-0.000043	0.000000*	0.000000*	0.000000*	0.030417*	0.194733	0.199036
250_min	-122.95328	0.000008	-2.033027	0.008029	0.000034	0.000000*	0.006928*	0.000000*	0.575463	0.744928	0.110887
250_max	-118.898613	0.000006	-2.185694	0.009526	0.00035	0.000000*	0.018575*	0.000000*	0.478889	0.000928*	0.152308
150_min	-122.221656	0.000005	-2.119851	0.012802	0.000045	0.000000*	0.008505*	0.000000*	0.545195	0.17214	0.127089
150_max	-122.755597	0.000005	-2.289917	0.013508	0.00027	0.000000*	0.007652*	0.000000*	0.116529	0.000224*	0.163509

Table 2. Summary of all the OLS Results.

Among explanatory variables, GWL was the most influential, with strong negative coefficients indicating deeper groundwater levels correlated with higher subsidence. In Hagonoy, the effects of GWL were weaker, likely due to local hydrogeological conditions or data limitations. Population density (POP) was positively associated with subsidence, particularly in Calumpit, reflecting urban pressure. BUV had minimal association with subsidence, although in some areas, denser infrastructure appeared to reduce subsidence, possibly due to stable ground.

The GWE variable showed unexpected positive coefficients, particularly in Calumpit, likely reflecting methodological issues or unmeasured variables. Additionally, inconsistencies in extraction data, such as unexplained jumps, may have influenced the model. GWE was excluded from the GWR analysis due to multicollinearity, which hindered localized model variation despite acceptable OLS multicollinearity diagnostics.

R^2 values ranged from 0.10 to 0.26, with the highest observed in Hagonoy using the 250m grid with minimum PSI velocities, suggesting that finer spatial stratification improves model fit. These findings emphasize the need for a GWR approach to better model spatially varying relationships and address nonstationarity in subsidence drivers.

3.4.3 GWR Model Results

3.4.3.1 GWR Model Performance Summary

GWR was applied with three predictors: GWL, POP, and BUV, excluding GWE due to multicollinearity. The GWR model achieved an adjusted R^2 of 0.94, explaining about 94% of subsidence variation, and a lower AICc of 1331.98 compared to 38,759.86 for the OLS model, which indicates a better fit.

Residual diagnostics supported the GWR model. The histogram of standardized residuals approximated a normal distribution, indicating a better fit than the OLS model. Global Moran's I analysis of GWR residuals yielded a Moran's Index of 0.008416, with a z-score of 4.90 and a p-value < 0.000001, which suggested minor spatial autocorrelation. However, this was significantly lower than OLS residuals, indicating the GWR model effectively reduced spatial autocorrelation and provided a more robust framework.

3.4.3.2 Interpretation of GWR Findings

The GWR analysis revealed more nuanced spatial patterns than the OLS models. GWL maintained a negative relationship with subsidence ($R^2 = 0.11$), supporting the hypothesis that groundwater depletion contributes to increased deformation. Built-up volume also showed a negative correlation ($R^2 = 0.06$), indicating urban development may exacerbate subsidence through loading effects and higher groundwater demand. Population density had a weak global relationship ($R^2 = 0.003$) but may influence subsidence locally.

While global scatterplots indicated weak linear relationships, the GWR model captured important localized effects, as shown by the higher adjusted R^2 and improved residual diagnostics. These results emphasized the benefits of spatially adaptive modeling for understanding subsidence patterns.

3.4.4 GWR Coefficient Maps

3.4.4.1 GWR Coefficient Maps (Full Dataset, Scaled)

This contribution has been peer-reviewed. The double-blind peer-review was conducted on the basis of the full paper.
https://doi.org/10.5194/isprs-annals-X-5-W4-2025-307-2026 | © Author(s) 2026. CC BY 4.0 License.

The GWR coefficient maps (Figure 13) showed spatial variability in the relationships between subsidence and its predictors. The intercept map (Figure 13a) highlighted baseline deformation, with higher values in southern Hagonoy. The GWL map (Figure 13b) showed strong negative relationships in southern Hagonoy, aligning with areas of intense groundwater extraction.

Population density (Figure 13c) and built-up volume (Figure 13d) indicated moderate positive effects in central Hagonoy and western Calumpit, suggesting urbanization contributes to subsidence. However, eastern Calumpit and northern Hagonoy show weaker or negative coefficients, indicating other unmodeled factors may be at play.

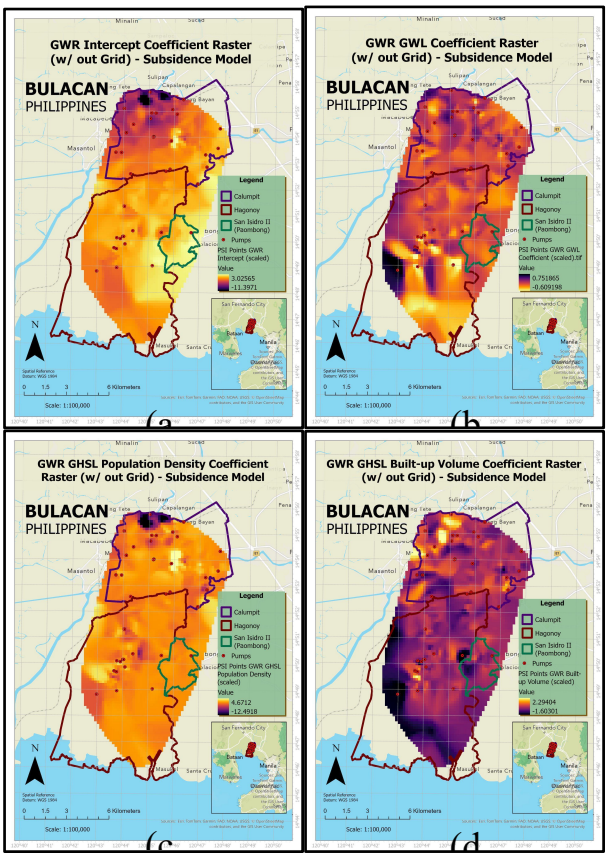

Figure 13. Scaled GWR coefficient maps showing local effects on subsidence: (a) intercept, (b) GWL, (c) POP, (d) BUV.

3.4.4.2 GWR Coefficient Maps (Grid-Based PSI Sampling, Scaled)

To reduce point-density bias, GWR was applied using a 250-meter fishnet grid with PSI minimum velocity points. This model achieved an adjusted R^2 of 0.88, showing strong spatial agreement with the full dataset. The grid-based GWR maps (Figure 14) confirmed southern Hagonoy as a subsidence hotspot, where groundwater depletion and urban load interact to drive deformation.

The intercept map (Figure 14a) and GWL map (Figure 14b) highlighted the importance of groundwater stress in southern Hagonoy. The population density (Figure 14c) and built-up volume (Figure 14d) maps showed strong positive influences in urban zones, though these effects are spatially varied.

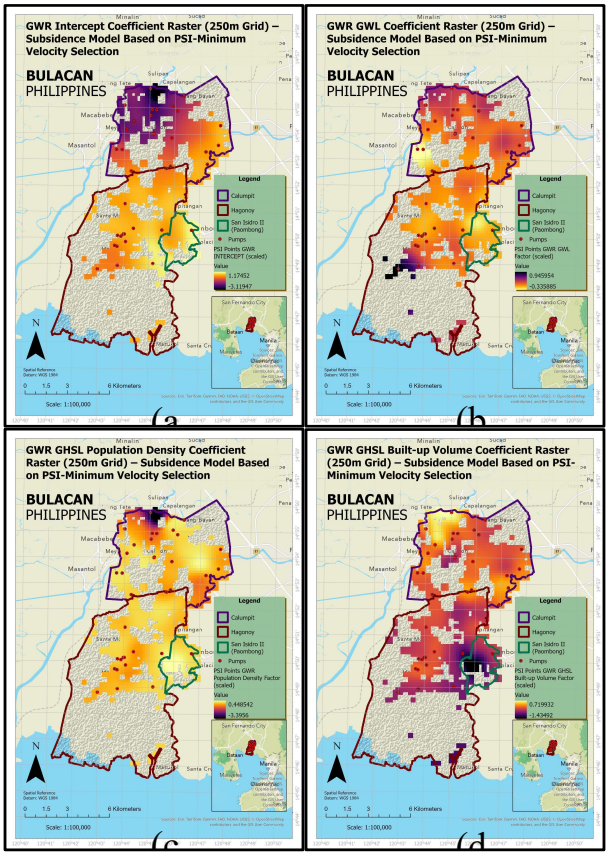

Figure 14. Scaled GWR coefficient rasters (250m grid): (a) intercept, (b) GWL, (c) POP, (d) BUV).

These spatially explicit results underscored the importance of considering local variations in drivers of land subsidence and validated the effectiveness of GWR in uncovering patterns that would otherwise be obscured in global regression models.

3.4.5 Zone-Based Subsidence Comparison and Cumulative Exposure Analysis

3.4.5.1 Welch's T-Test Between Extraction and Non-Extraction Zones

PSI points were categorized into two zones: Zone A (within 500 meters of active pumping stations) and Zone B (beyond 500 meters). Welch's t-tests revealed consistently higher subsidence in Zone A. In Hagonoy, average subsidence in Zone A was -60.31 mm/year versus -57.69 mm/year in Zone B, while Calumpit showed a greater difference between the two zones of about 6.13 mm/year. Across the study area, the gap between Zones A and B was 4.91 mm/year ($p < 0.001$). These results confirmed that proximity to pumping stations significantly influences land deformation and can inform the delineation of high-priority monitoring zones.

3.4.5.2 Linear Proximity Zoning

Using 250-meter increments from pumping stations (PZ1–PZ5), subsidence was strongest in the zones closest to extraction points (PZ1 and PZ2). One-way ANOVA confirmed significant differences among zones ($F = 40.61$, $p < 0.001$), with post hoc tests indicating that PZ1 exceeded PZ4 and PZ5 by 5–7 mm/year. This clear spatial gradient demonstrated that subsidence effects decay with increasing distance from pumping centers, underscoring the localized nature of extraction impacts.

This contribution has been peer-reviewed. The double-blind peer-review was conducted on the basis of the full paper.
https://doi.org/10.5194/isprs-annals-X-5-W4-2025-307-2026 | © Author(s) 2026. CC BY 4.0 License.

3.4.5.3 Non-Linear Proximity Zoning

To better reflect the rapid spatial decay of extraction impacts, subsidence points were grouped into non-linear interval distances from pumping stations: 0–100 m (PZ1), 101–300 m (PZ2), 301–600 m (PZ3), 601–1000 m (PZ4), and >1000 m (PZ5). Results showed that subsidence was highest within the immediate vicinity (PZ1) and decreased progressively with distance. One-way ANOVA indicated significant variation among zones ($F = 39.10$, $p < 0.001$), with post hoc tests confirming PZ1 exceeded PZ4 and PZ5 by 7–8 mm/year. This non-linear pattern highlighted that extraction effects are most pronounced within the first 600 meters of the pumping stations.

3.4.5.4 Summary

Zone-based and proximity-driven analyses consistently demonstrated that groundwater extraction exerts a localized but measurable influence on land subsidence. Statistical testing (Welch's t-test) confirmed that areas within 500 meters of pumping stations experience significantly greater deformation than farther zones, underscoring proximity as a critical factor. Both linear and non-linear zoning reinforced this pattern, with the steepest subsidence gradients occurring within the first few hundred meters of extraction points. Linear zoning highlighted a clear stepwise decay in deformation across successive distance bands, while non-linear zoning captured the sharper decline in impacts within 600 meters of pumping stations. Collectively, these findings established empirical evidence that subsidence risk is spatially concentrated near pumping centers, which provided a basis for delineating high-priority monitoring zones, designing buffer areas, and implementing targeted regulatory controls to protect groundwater-dependent communities.

4. Conclusions and Recommendations

This study examined the relationship between land subsidence, groundwater extraction, and urbanization in Hagonoy and Calumpit, Bulacan, from 2015 to 2021-Q1. By integrating Sentinel-1 PSI-derived deformation data, spatial regression techniques, and GNSS-based field validation, the analysis confirmed that groundwater withdrawal and urban development are significant drivers of ground deformation in the study area. The GWR model ($R^2 = 0.88$) underscored the importance of accounting for spatial variability, with built-up volume and groundwater level emerging as the strongest predictors of subsidence. In contrast, population density showed weaker and less consistent effects, reflecting the limitations of coarse demographic datasets.

Zonal analyses further revealed that areas within 500 meters of pumping stations experienced significantly higher subsidence rates. Mean subsidence rate reached -70.22 mm/year in Zone A compared to -65.31 mm/year in Zone B, while post hoc tests identified differences exceeding 5–7 mm/year between pumping zones, across the study area. GNSS surveys correlated strongly ($R^2 = 0.70$) with PSI-derived velocities, affirming the reliability of satellite-based monitoring. Overall, the findings demonstrate that spatial proximity to extraction wells, groundwater depth, and urbanization intensity are key contributors to the observed land subsidence patterns in Hagonoy and Calumpit.

Moving forward, addressing data gaps will be critical. More detailed well-level extraction records and barangay-level census data should be incorporated to refine urbanization and groundwater stress modeling. Expanding GNSS validation networks and conducting regular re-surveys would further strengthen the reliability of InSAR-derived subsidence measurements. Importantly, localized spatial models such as GWR should be adopted more widely to detect and anticipate emerging hotspots.

Finally, the study highlights the urgent need to integrate subsidence risk into municipal planning, land-use zoning, and groundwater permitting. Current databases maintained by the Local Water Utilities Administration (LWUA) and the NWRB lack well-level extraction volumes and monitoring mechanisms, limiting effective oversight. Establishing detailed reporting systems, coupled with stricter compliance and verification of extraction limits, will be essential to mitigate further land deformation. By bridging satellite-based science with local governance, this study provides evidence-based insights that can guide sustainable water resource management and urban planning in subsidence-prone regions.

Acknowledgements

We extend our sincere gratitude to Dr. Philip Minderhoud, LWUA, NAMRIA, the Hagonoy and Calumpit Water Districts for their invaluable support throughout our research.

References

Cos, W., 2022. Life in the sinking neighborhoods of Bulacan. ABS-CBN News. Retrieved November 2024, from www.abs-cbn.com/specials/bulacan- sinking.

Dang, V.K., Doubre, C., Weber, C., Gourmelen, N., Masson, F., 2014. Recent land subsidence caused by the rapid urban development in the Hanoi region (Vietnam) using ALOS InSAR data. *Natural Hazards and Earth System Sciences,* 14 (3), pp. 657-674, doi.org/10.5194/nhess-14-657-2014.

European Commission [EC], Joint Research Centre [JRC], 2021a. Assessing changes in subsidence rates in the low Pampanga river basin and Manila area, Philippines (2021-04-30) (A/2) [Dataset]. *European Commission*. data.europa.eu/89h/e47cad9f-70c8-4d29-b5d6-d1b89f6ebc9d.

European Commission [EC] & Joint Research Centre [JRC], 2021b. GHSL data package 2023. *Publications Office of the European Union.* doi/10.2760/098587.

Fresco, T.A., 2012. Integrated River Management Models: Implications for Collaborative Governance and Management of the Angat River Basin, Philippines. doi.org/10.14288/1.0102550.

Lagos, D., Rebadolla, J., Anne, F., Farin, F. A. B., & Eco, R., 2023. Flooding and Subsidence Research: Bulacan Province, Northern Manila Bay Area, Philippines. Retrieved February 2025, from www.researchgate.net/publication/369742698_Flooding_and_Subsidence_Research_Bulacan_Province_Northern_Manila_Bay_Area_Philippines.

NOAA., 2024. What is subsidence? National Ocean Service website. Retrieved November 2024, from oceanservice.noaa.gov/facts/subsidence.html.

Velis, M., Conti, K. I., & Biermann, F., 2017. Groundwater and human development: synergies and trade-offs within the context of the sustainable development goals. *Sustainability Science*, 12(6), 1007–1017. doi.org/10.1007/s11625-017-0490-9.